inorganics

MDPI

Article

Biosynthesized ZnO-CuO Nanocomposite for Biofilm Formation of *Proteus mirabilis*upon *LuxS* Gene Expression

Mais Emad. Ahmed [1,*], Noor Hamza Faiq [1], Hayfa Habes Almutairi [2] and Mir Waqas Alam [3,*]

[1] Department of Biology, College of Sciences, University of Baghdad, Baghdad, Iraq; nour.hamza1102a@sc.uobaghdad.edu.iq
[2] Department of Chemistry, College of Science, King Faisal University, Al-Ahsa 31982, Saudi Arabia; halmutairi@kfu.edu.sa
[3] Department of Physics, College of Science, King Faisal University, Al-Ahsa 31982, Saudi Arabia
* Correspondence: mais.emad@sc.uobaghdad.edu.iq (M.E.A.); wmir@kfu.edu.sa (M.W.A.)

Abstract: *Proteus mirabilis* has been identified as the third most frequent reason for catheter-associated urinary tract infections. The production of urease significantly enhances the force of catheter blockage caused by biofilm formation. Because biofilms are important virulence factors that make antibiotics less potent, it is becoming increasingly important to develop novel alternative antibiotics. In addition to the unique properties they possess, nanoparticles made from metal oxide are currently attracting considerable attention as possible antibacterials. This research aims to explore the potential anti-biofilm properties of green manufactured ZnO-CuO nanoparticles generated by *P. mirabilis*. By synthesizing reductive enzymes, bacterial cells can participate in the biosynthesis process. This study explores whether green synthesized ZnO-CuO nanoparticles can work as an anti-biofilm agent formed by *P. mirabilis*. These nanoparticles were generated using Bacteriocins to determine their effectiveness against bacteria, which were partially purified and showed antimicrobial activity against Gram-negative bacteria of *P. mirabilis*. AFM, TEM, FESEM, XRD, and ultraviolet (UV)–visible spectroscopy were used to analyze the biosynthesized nanoparticles to ascertain their chemical and physical characteristics. XRD verified the hexagonal structure, TEM demonstrated a size range of 96.00 nm, and FESEM verified the surface morphology. The dispersion and roughness of the nanoparticles are shown through AFM examination. The produced nanoparticles' UV-visible spectra displayed a maximum peak at 287 and 232 nm. When applied to strains (wild-type) of *Proteus mirabilis* (multidrug-resistant), copper and zinc nanoparticles had notable biofilm inhibitory effects. Weak biofilm production has been demonstrated by bacteria that effectively generate biofilms, following incubation with 128 µg/mL subminimum inhibitory concentrations (MICs) of CuO nanoparticles for 24 and 48 h at 37 °C. Following treatment with the ZnO-CuO nanocomposite of these strains, downregulation alterations in *LuxS* expression were detected by utilizing a real-time PCR process. After this, isolates were treated with the nanocomposite, and downregulated shifts in *LuxS* expression were found by utilizing the real-time PCR technique in contrast with the isolates that were not treated. Zinc oxide (ZnO) nanoparticles can be utilized as antibacterial agents in a concentration-dependent manner, aligning with all observed findings. The present research demonstrates that green synthesized copper oxide–zinc oxide nanocomposites are effective anti-biofilm agents against *P. mirabilis*. Their noteworthy downregulation of *LuxS* gene expression successfully prevents biofilm formation and swarming motility.

Keywords: *Proteus mirabilis*; anti-biofilm; ZnO-CuO nanocomposite; *LuxS* gene

check for updates

Academic Editor: Vladimir Arion

Received: 23 January 2025
Revised: 12 February 2025
Accepted: 16 February 2025
Published: 19 February 2025

Citation: Ahmed, M.E.; Hamza Faiq, N.; Almutairi, H.H.; Alam, M.W. Biosynthesized ZnO-CuO Nanocomposite for Biofilm Formation of *Proteus mirabilis*upon *LuxS* Gene Expression. *Inorganics* **2025**, *13*, 65. https://doi.org/10.3390/inorganics13020065

Copyright: © 2025 by the authors. Licensee MDPI, Basel, Switzerland. This article is an open access article distributed under the terms and conditions of the Creative Commons Attribution (CC BY) license (https://creativecommons.org/licenses/by/4.0/).

1. Introduction

Bacterial cells are normally located in the form of sessile aggregates known as biofilms, which are polymicrobial and can generate slimy Extracellular Polymeric Substances (EPSs). EPSs are commonly referred to as a biofilm matrix and are a heterogeneous repository of various biomolecules such as a combination of polyproteins and extracellular DNA/RNA [1]. Because they can boost bacterial resistance to planktonic cells by up to 1000 times, bacterial biofilms are common in clinical settings. Despite the use of preventative measures in hospitals and other therapeutic settings, nosocomial infections continue to cause a significant rate of morbidity and mortality [2].

The complex communication throughout the biofilm community allows bacteria to resist various stressors, drugs, and host defense mechanisms [3]. Bacteria generate complex multicellular communities called biofilms, and the extracellular polymer substances that make up these communities can be characterized as either surface-attached or non-surface-attached aggregates. Biofilms can be created from a wide range of bacterial species that are present in living environments or hosts [4]. In such a situation, researchers have made efforts to provide new alternatives to traditional antibiotic treatment that can successfully combat multidrug resistance (MDR) and biofilm-producing bacteria. *P. mirabilis* is frequently implicated in the occurrence of intricate urinary tract infections (UTIs) among individuals with anatomical or functional abnormalities [5]. *P. mirabilis* is an opportunistic pathogen that has been linked to several hospital-acquired and community-acquired diseases that are hard to control because they are not susceptible to many antibiotics. The ability of *P. mirabilis* to form biofilms and adapt to various environments further complicates treatment options, making it a significant concern in healthcare settings. As research continues to unveil the mechanisms behind its resistance and adaptability, there is a pressing need for novel therapeutic strategies and improved infection control measures. Addressing the challenges posed by *P. mirabilis* will be crucial in reducing its impact on patient outcomes and overall healthcare efficacy. Moreover, collaboration between researchers, healthcare professionals, and policymakers is essential in order to develop comprehensive approaches that can effectively combat this opportunistic pathogen. By prioritizing education and awareness, the healthcare community can better equip itself to manage infections caused by *P. mirabilis* and similar resistant organisms.

Researchers are making efforts in this evolving setting for the future with alternative antibiotic treatment that efficiently fights against bacteria that create biofilms and induce multidrug resistance (MDR).

The green synthesis of nanomaterials has garnered considerable attention as a sustainable, useful, reliable, economical, abundant, and environmentally friendly paradigm. Green synthesis could perhaps be a sophisticated tool to decrease the toxic effects associated with conventional synthesis procedures that are generally selected in industry and testing facilities for nanomaterials [6]. This is a sustainable method for the production of green NPs via the use of Streptomyces albogriseolus cell-free supernatant as a stabilizing and reducing agent. The longest absorption peak of the biosynthesized GNPs appears at 540 nm.

On TEM images, GNPs were spherical in shape and ranged in size from 5.42 to 13.34 nm. The size and shape of the biosynthesized nanoparticles with the highest yield were assessed with TEM evaluation. The TEM image showed that the biosynthesized GNPs of Panax ginseng leaves primarily have spherical shapes with particle sizes in the range of 3.41–14.5. The biosynthesized nanoparticles showed the formation of well-dispersed spherical GNPs with sizes that range from 5.42 to 13.34 nm [7].

One of the most significant semiconductor metal oxide nanoparticles is zinc oxide (ZnO), a special inorganic substance with a variety of biological uses (anti-inflammatory and antibacterial). Quorum sensing (QS) is the mechanism that makes microbial commu-

nication possible. It depends on environmental signaling molecules being continuously released. QS's main task is to manage essential cellular functions like the synthesis of virulence factors and the creation of biofilms. Alternative antimicrobial therapies must be found because bacteria are still becoming resistant to overused antibiotics [8]. To create antimicrobials that can attack virulence factors without harming mammalian cells, researchers are exploring nanotechnology. As antioxidant, antifungal, and antibacterial agents with anticancer characteristics in a variety of applications, metal nanoparticles manufactured by employing microorganisms have proven to be a unique solution for physical and chemical techniques [9]. Metallic nanoparticles (CuNPs) and zinc oxide nanoparticles (ZnONPs) produced through green synthesis can be used as antimicrobials to kill plant-infectious microbes [10]. These results are similar to those of earlier research that showed that CuO NPs could break down biofilms and change gene expression levels. In one study, CuO and ZnO nanoparticles were able to lower the total amount of QS molecules (like AHL and AI-2) in the biofilm matrix. They also stopped these QS-related genes from being expressed. The levels of expression of important genes that controlled the QS process, like *LuxS* and LsrK, went up significantly after being exposed to CuO NPs compared to the control group in a different study [11]. Although no studies have been conducted to investigate the effect of ZnO-CuO nanocomposites on the gene expression of *LuxS* in *P. mirabilis*, it should be noted that other nanoparticles have been used to target other genes involved in quorum sensing regulation in this species. As a result, this study could be the first to investigate the potential effect of nanocomposites on these genes. ZnO/CuO nanocomposites produced using the green synthesis method are a novel outcome to be reported from *Proteus mirabilis*. Zinc and copper electrodes were used to produce nanocomposites characterized through the use of sophisticated characterization techniques [12,13]. This study presents a novel approach to the biosynthesis of ZnO-CuO nanocomposites using a microbial method that enhances nanoparticle stability, bioavailability, and antibacterial efficiency. By targeting MDR *Proteus mirabilis*, a key pathogen in biofilm-related infections, this work not only demonstrates potent antimicrobial effects but also reveals a previously unexplored mechanism of quorum sensing disruption through *LuxS* gene regulation. The findings provide a sustainable and scalable strategy for developing advanced antibacterial nanomaterials, offering promising applications in biomedical and environmental fields.

2. Results and Discussion

2.1. Isolation and Identification

Between September and December 2021, a total of 130 specimens were gathered from various urine sources, including catheter urine (50) and urine samples from UTI patients (80). Each material was inoculated directly into blood agar and MacConkey agar plates. As seen in Table 1 below, only 60 (46%) of the total specimens were determined to be *P. mirabilis*. Additionally, it was determined that 38 (47.5%) of the cultured urine samples were *P. mirabilis* strains. Furthermore, *P. mirabilis* was found in 22 (44%) of the cultures of catheter urine samples. On the basis of the colony's size, shape, color, texture, and swarming behavior, preliminary diagnoses were made. *P. mirabilis* appeared as a swarming phenomenon on blood agar plates and as a pale colony on MacConkey agar after overnight incubation at 37 °C (Figure 1).

Table 1. Occurrence of *P. mirabilis* isolates in clinical samples.

No. of *Proteus* spp. (%)	No. (%) of *P. mirabilis*	Number of Samples	Sample Source
8 (10%)	38 (47.5%)	80	Urine
5 (6.2%)	22 (44%)	50	Catheter urine
13 (10.19%)	60 (46%)	130	Total

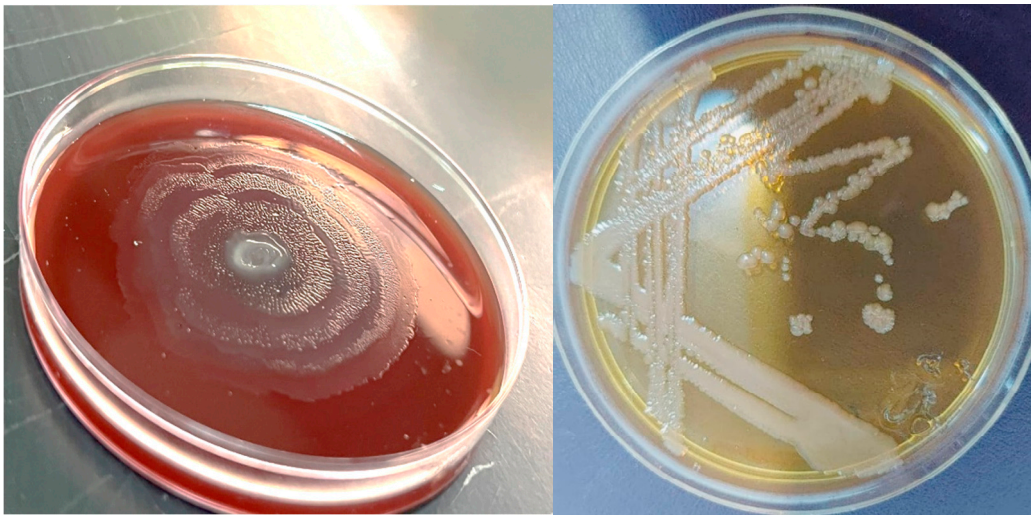

(**a**) (**b**)

Figure 1. (**a**) *P. mirabilis* on MacConkey agar and (**b**) *P. mirabilis* on the blood agar at 37 °C for 24 h.

2.2. Susceptibility Testing of the Antibiotic MDR Strains Screened

It emerged that 40 out of 64 isolates (62.5%) were MDR strains, following a period of incubation of 24 h at 37 °C. All of the tested isolates exhibited resistance to piperacillin–tazobactam, 6 isolates (15%) were found to be resistant to levofloxacin, and 6 isolates (15%) exhibited resistance to ciprofloxacin. Fifteen isolates (37.5%) did not exhibit growth inhibition by ampicillin, two strains (5%) and six isolates (15%) did not exhibit growth inhibition by cefoxitin, and 17 isolates (42.5%) did not exhibit growth inhibition by nitrofurantoin (Figure 2).

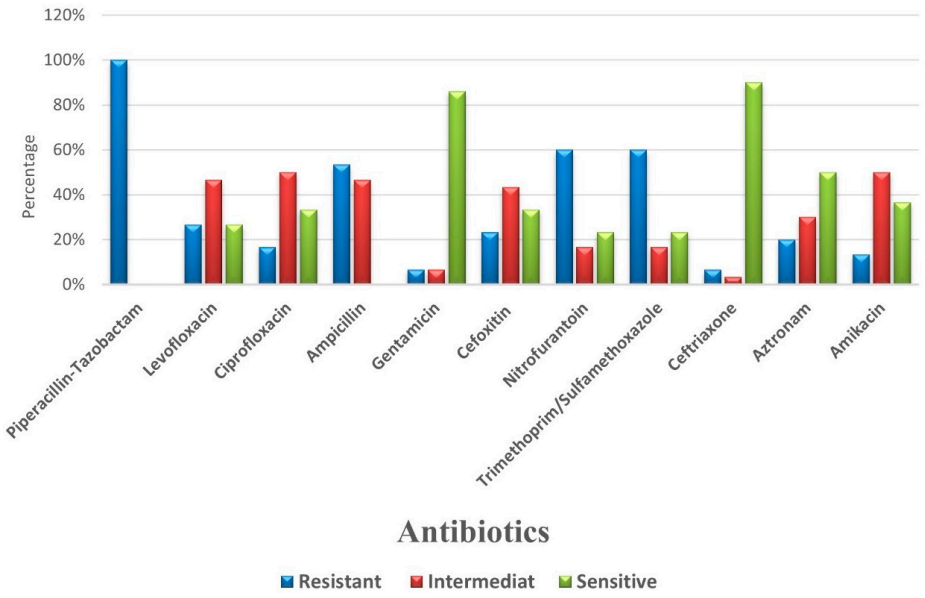

Figure 2. Percentage of antibiotic susceptibility among *P. mirabilis*isolates.

2.3. Biofilm Formation of *P. mirabilis*

All 60 isolates had their *P. mirabilis* biofilm formation evaluated, and the findings confirmed that every isolate developed biofilm. Twenty (33.3%) isolates had strong biofilm production; all of these isolates came from samples gathered from patients' indwelling catheters. Twenty-two (36.6%) isolates experienced moderate biofilm production and eighteen (30%) isolates had weak production of biofilm (Figure 3 and Table 2).

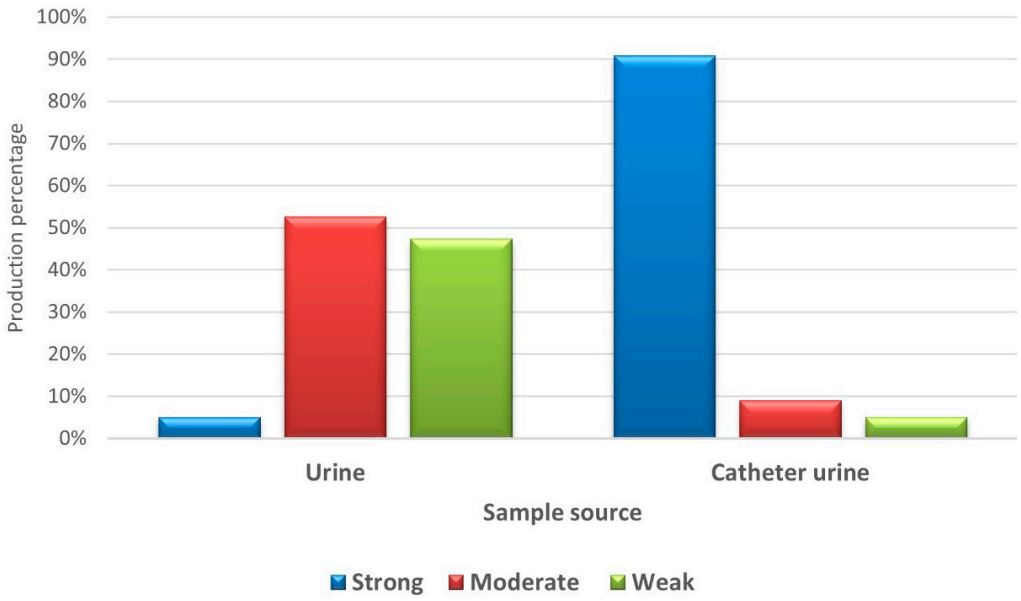

Figure 3. Percentage of biofilm per microtiter plate for *P. mirabilis*isolates according to urine source.

Table 2. Biofilm formation of isolates of *P. mirabilis.*

Isolate Code	O.D	Biofilm Production
P.m1	3.1	Moderate
P.m2	1.6	Weak
P.m3	1.8	Weak
P.m4	2.15	Moderate
P.m5	1.36	Weak
P.m6	1.8	Weak
P.m7	1.77	Weak
P.m8	3.96	Moderate
P.m9	1.34	Weak
P.m10	2.125	Moderate
P.m11	2.24	Moderate
P.m12	4.90	Strong
P.m13	2.60	Moderate
P.m14	5.75	Strong
P.m15	2.42	Moderate
P.m16	1.88	Weak
P.m17	9.19	Weak
P.m18	6.30	Strong
P.m19	2.60	Weak
P.m20	7.15	Strong

2.4. Biosynthesis of ZnO-CuO Nanoparticles

P. mirabilis isolates were used to biosynthesize the nanocomposite. Besides generating light blue precipitates, the color changed to blue from yellow, indicating the development

of nanoparticles. The precipitate had a greenish–blue appearance upon centrifugation. Following microwave drying, a gleaming blue powder was produced (Figure 4).

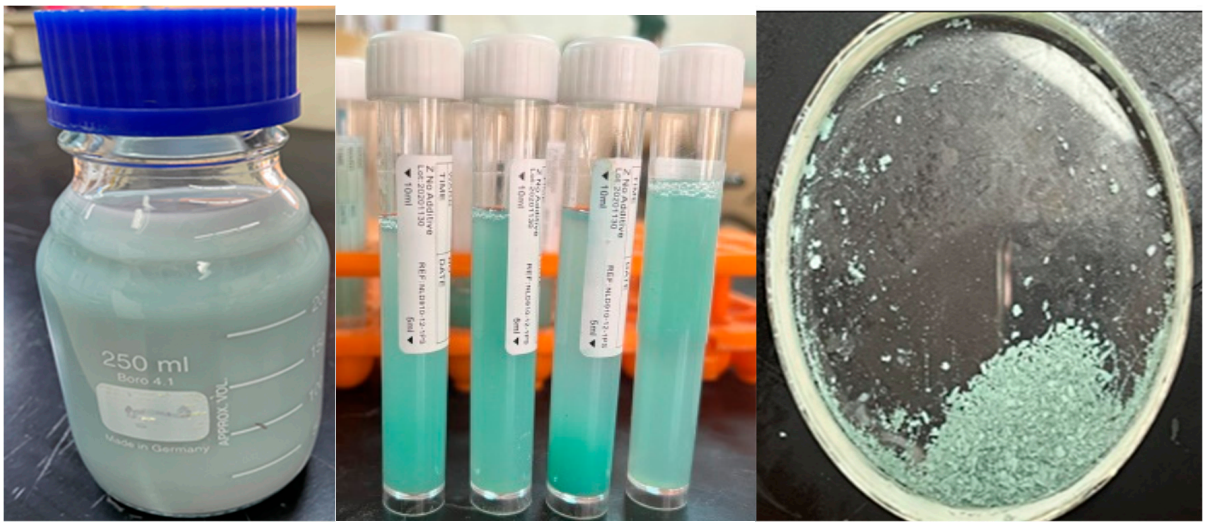

Figure 4. Biosynthesis of CuO-ZnO nanocomposite powder.

2.5. Characterization Techniques for Nanocomposites

2.5.1. UV–Vis Spectroscopic Analysis

The compound was dissolved in de-ionized water for standard analysis. The formation of ZnO and CuO was confirmed by the information available. The CuO-ZnO NPs that were biosynthesized showed absorption at 232 nm and 287 nm (Figure 5). By comparing the UV-Vis absorption peaks at 232 nm and 287 nm with those noted in a previous study, the results were close to the previous reports [14], showing a biogenic $ZnO/CuO/Fe_2O_3$ nanocomposite through the use of an aqueous *Ocimum basilicum* L. leaf extract. $ZnO/CuO/Fe_2O_3$ NC production was demonstrated through UV-visible spectrophotometry, which confirmed biosynthesis. The visible range absorption spectra show a peak at λ_{max} in the nanometer range.

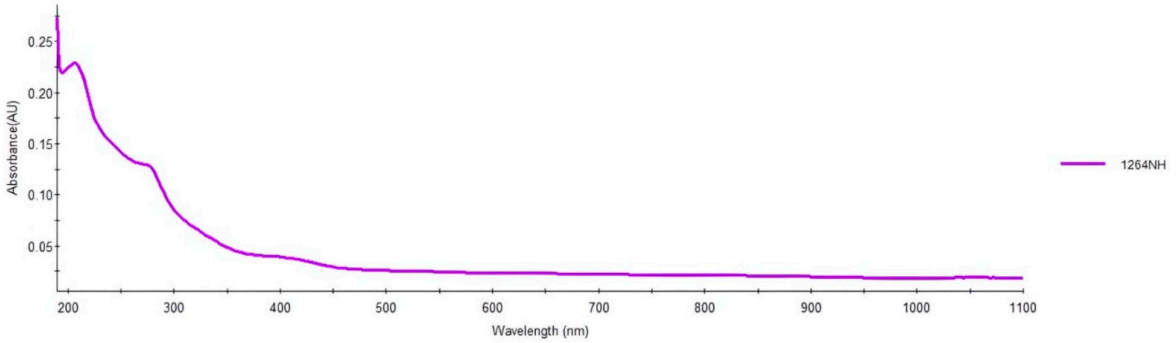

Figure 5. UV–visible spectra of nanocomposite CuO-ZnO NPs.

2.5.2. Atomic Force Microscopy (AFM) Analysis

The CuO-ZnO NPs were subjected to AFM analysis using CSPM in order to detect and describe the nanoparticle distributions. The mean square roughness and estimated particle size were calculated. The average grain size of the nanoparticles was 96.00 nm, as can be seen in the three-dimensional profile of the nanocomposite in Figure 6. To gain a better understanding of the topography and roughness of the 1.93 µm, 3.3 µm, and 3.46 µm nanoparticles, several magnification ranges were used.

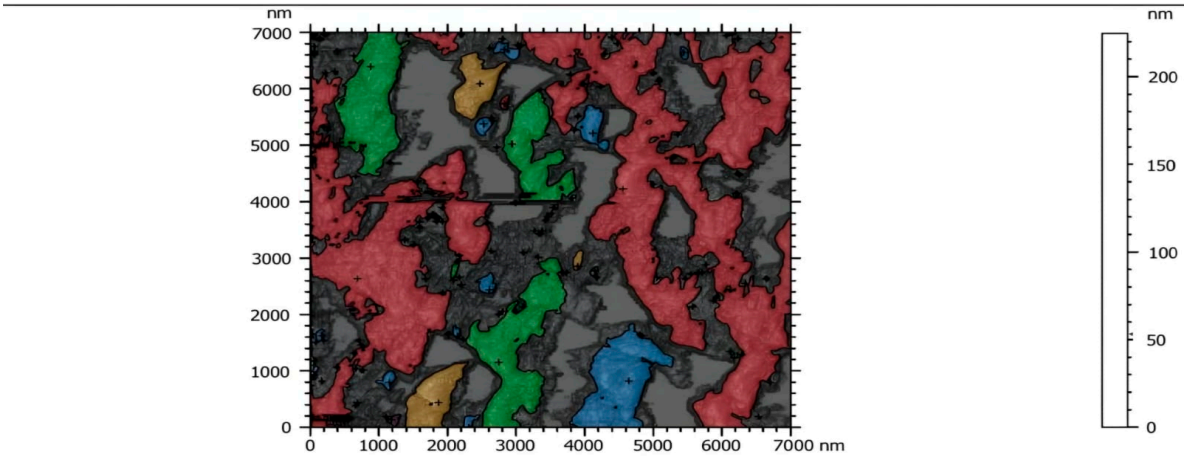

Information		
Method	Threshold detection	
Channel	Deflection - Scan forward (1 / 4)	
Threshold 1	53.46	nm
Number of particles	222	
Coverage	48.37	%
Density	4530612	Particles/mm²

Parameters	Projected area	Mean diameter	Minimum diameter	Maximum diameter	Z-maximum
Unit	nm²	nm	nm	nm	nm
Particle #1	5663	70.08	78.92	95.23	63.19
Particle #2	5663	70.08	78.92	95.23	63.19
Particle #3	879.1	19.94	20.54	48.46	57.17
Particle #4	1578037	1276	680.0	2554	142.1
Particle #5	1491	27.81	34.88	57.67	58.76
Mean	107592	96.00	65.05	181.8	61.84

Bear

Figure 6. AFM analysis of the CuO-ZnO nanocomposite.

2.5.3. Transmission Electron Microscopy (TEM) Analysis

The size and shape of the nanocomposites were investigated using TEM imaging. TEM assessment supports analysis of the nanoparticles' core structure. The TEM images (Figure 7) show agglomeration, with the formation of particles with spherical and semi-spherical geometries. The TEM images demonstrate the spherical shape of CuO-ZnO NPs, which are created by oxidizing copper and zinc ions by utilizing the *P. mirabilis* filtrate.

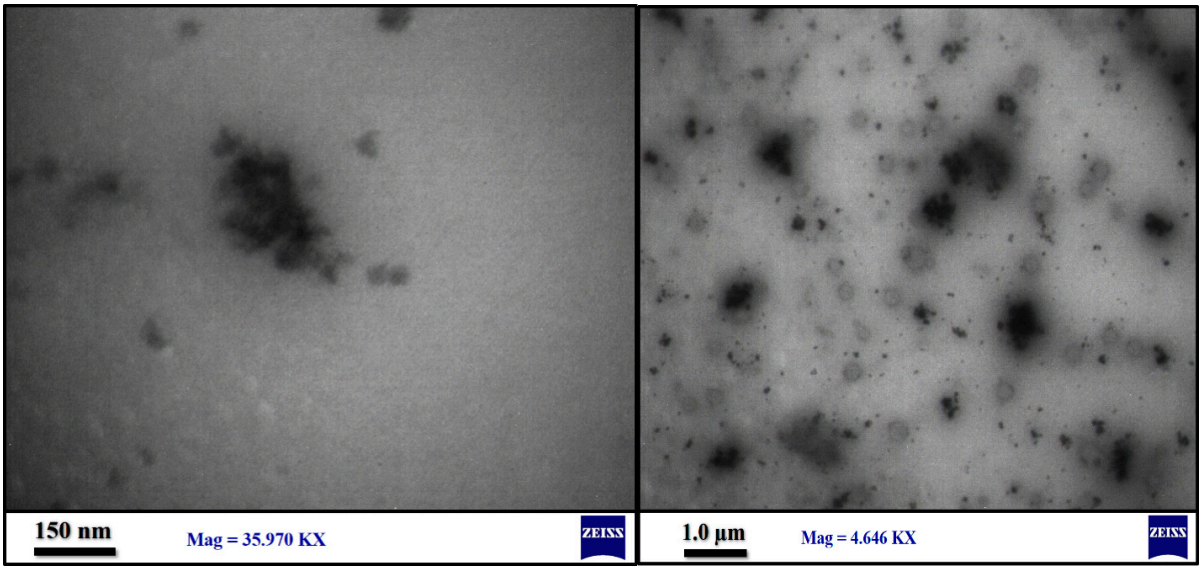

Figure 7. TEM images of Cu-Zn NPs.

2.5.4. Scanning Electron Microscopy (SEM)

The surface shape and properties of the produced nanoparticles can be examined with scanning electron microscopy (SEM). The green synthesized CuO/ZnO NC's morphology was determined through FE-SEM analysis, which suggested that the NPs were less than 100 nm in size. This indicated that the synthesis of CuO/ZnO NPs was successful since the synthesized NC's size ranged from 33.3 nm, including spherical and rod morphologies.

Further data about the outer morphology of the CuO-ZnO NPs was obtained via scanning electron microscopy (SEM). The CuO-ZnO NPs were arranged together and resembled merged cauliflowers, depending on the images (Figure 8). Higher magnification for further analysis revealed that these crowded NPs are aggregates of smaller copper and zinc nanoparticles with good homogeneity and sphere-like morphologies.

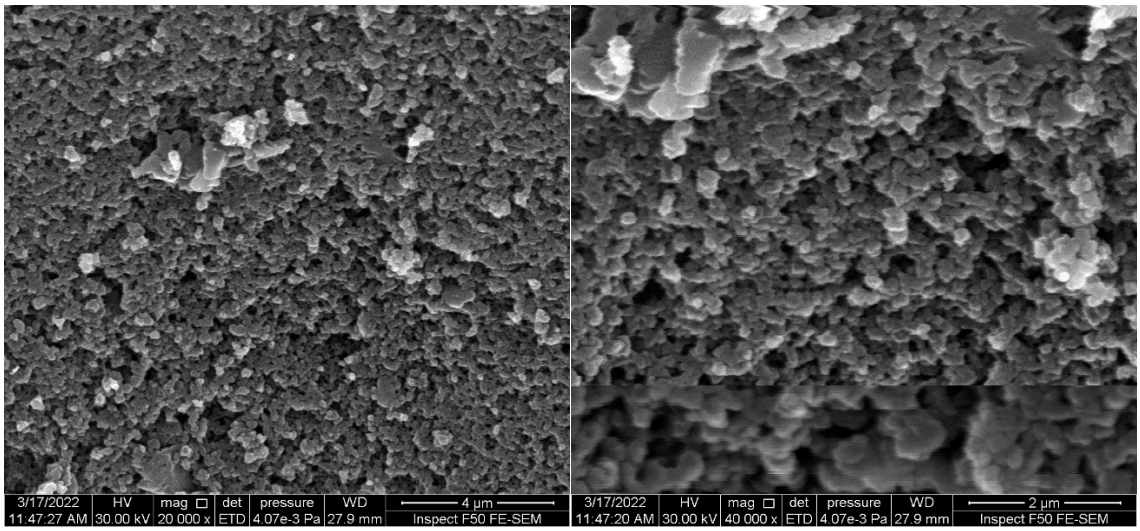

Figure 8. FESEM images with 60,000× and 15,000× magnification powers.

2.5.5. X-Ray Diffraction (XRD) Analysis

Dispersive X-ray diffraction was utilized to examine the crystalline structure and purity of the produced nanoparticles (NPs). The XRD spectra of Cu-Zn NPs are shown in Figure 9. The significant peaks that matched the diffraction peaks at 2θ values were revealed, showing the existence of Cu-Zn NPs: 11.794, 13.056, 16.766, 18.12, 19.525, 20.539, 22.494, 24.312, 35.725, 39.148, 42.864, 54.37, 57.254, 58.473, 59.689, 61.492, 72.206, 73.681, and 77.314. The wurtzite hexagonal phase was used to index all peaks in reference to JCPDS file No. 79-0207. Except for the unique spikes associated with the wurtzite-hexa phase of CuO-ZnO, there are no peaks in the spectrum associated with any impurities or bulk leftover materials found, demonstrating the exceptional purity of the generated uncapped NPs' physical phase.

2.5.6. Energy-Dispersive X-Ray Spectrometry (EDX)

The components of CuO-ZnO nanoparticles were analyzed by using an Energy-dispersive X-ray (EDX) spectrometer. Both qualitative and quantitative evaluations of the components that involved in the manufacturing of nanoparticles were performed through EDX analysis. The highest possible values for copper (Cu) and zinc (Zn) were obtained from the EDX analysis, indicating the pristine nature of the produced Cuo-Zno NPs. The Cu content was found to be 55.47 weight percent, indicating that the generated nanoparticles were in the purest form possible with few chemicals. The EDX spectra are displayed together with the composition percentage and the main elemental peak at 8 keV related to the Cu metal (Figure 10).

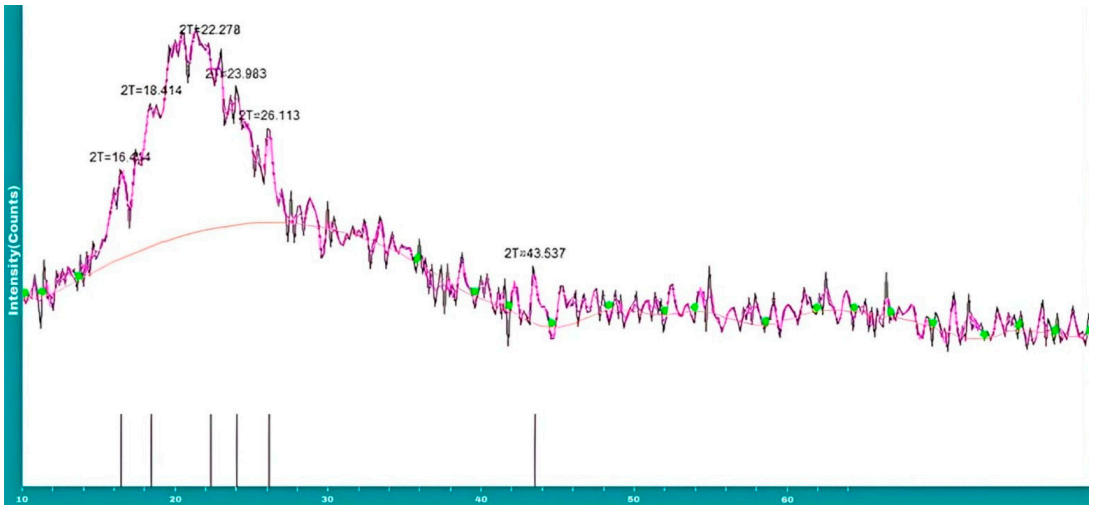

Figure 9. X-ray diffraction (XRD) spectra of the CuO-ZnO nanocomposites show 19 peaks at 2θ values.

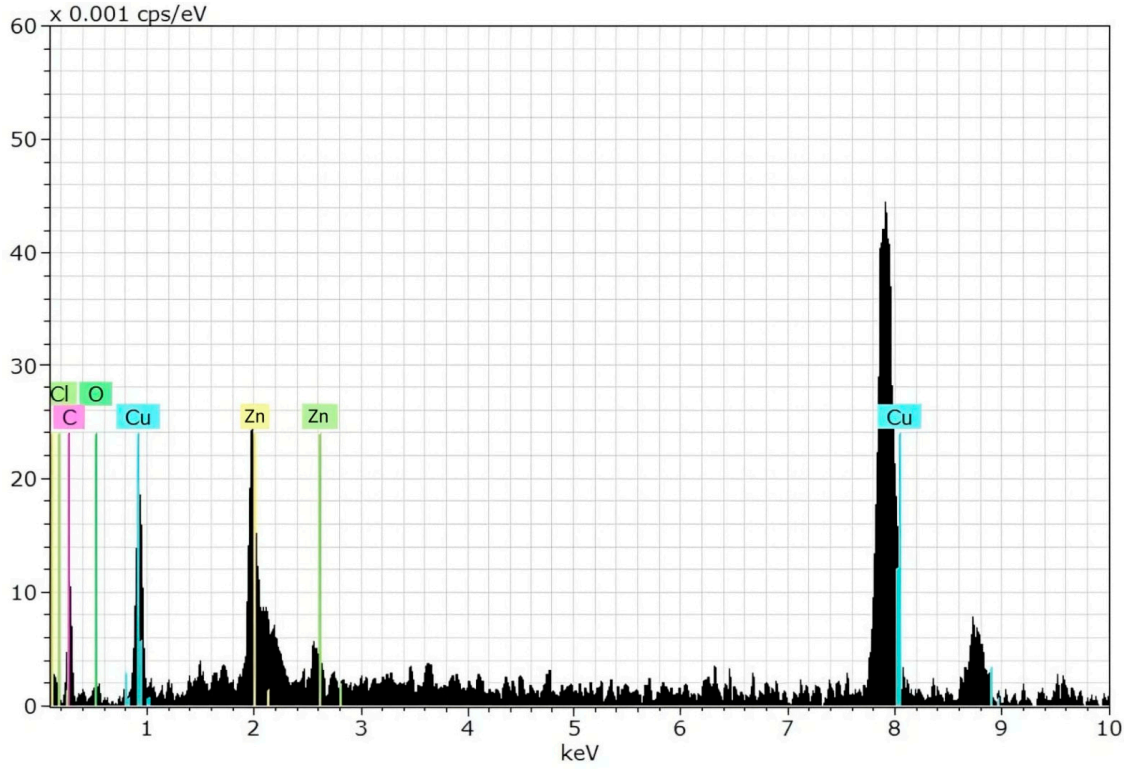

Figure 10. Energy-dispersive X-ray spectrometry of CuO-ZnO nanocomposites.

2.6. Minimum Inhibitory Concentration (MIC) of CuO-ZnO NPs

Following extensive analysis of NP synthesis, morphology, and minimum inhibitory concentration (MIC), quantitatively expressed in unit of micrograms per milliliter (µg/mL), the MIC of the CuO–ZnO NPs against the strong biofilm producer *P. mirabilis* isolates was found (P.m12, P.m14, P.m18, and P.m20) (Tables 3 and 4). Serial dilutions of each nanoparticle (2, 4, 8, 16, 32, 64, 128, and 256) µg/mL were poured into a tube of bacterial broth. The results displayed in Table 3 indicate that the different MIC concentrations of CuO-ZnO nanoparticles had a major effect on the viability of bacterial cells and resulted in a rate of 100% at 256 µg/mL where as the Sub-MIC was 128 µg/mL. The Sub-MIC of every nanoparticle was used to determine the inhibitory effect on biofilm formation.

Table 3. The minimal inhibitory concentration of CuO-ZnO NPs.

Isolate Code	MIC of CuO NPs and CuO-ZnO NPs (µg/mL)	Sub-MIC of CuO NPs and CuO-ZnO NPs (µg/mL)
P.m12	256	128
P.m14	256	128
P.m18	256	128
P.m20	256	128

Table 4. Anti-biofilm activity of the Sub-MIC of CuO -ZnO NPs.

Isolate Code	OD Before Treatment	OD After Treatment with CuO-ZnO NPs	Inhibition Perc.
P.m12	9.19	1.97	78.5%
P.m14	6.30	1.23	80.4%
P.m18	7.25	1.08	85.1%
P.m20	7.15	1.23	80.7%

2.7. Anti-Biofilm Activity of CuO-ZnO NPs

The anti-biofilm activity of ZnO-CuO nanoparticles was evaluated by assessing their effect on *Proteus mirabilis* biofilm formation at the sub-minimum inhibitory concentrations (Sub-MICs). The results indicate that biofilm inhibition varied depending on the Sub-MIC used. Using a plastic microtiter plate assay, nine isolates of *P. mirabilis* were identified as strong biofilm producers based on their optical density (OD) values measured at 630 nm. Among them, four isolates (P.m12, P.m14, P.m18, and P.m20) exhibited the highest biofilm-forming capacity, with P.m18 showing the strongest biofilm formation (OD = 7.25), followed by P.m20 (OD = 7.15). Following treatment with ZnO-CuO nanoparticles at the Sub-MICs, the ability of the four strongest biofilm-producing isolates to form biofilms was significantly reduced after 24 h of incubation at 37 °C. The OD values of these isolates showed a notable decline, indicating a decrease in biofilm mass. After 48 h of treatment, biofilm production was further inhibited, and the OD values of the *P. mirabilis* strains decreased from strong biofilm production to weak biofilm formation. Table 5 summarizes the biofilm inhibition percentages observed for the four selected *P. mirabilis* isolates. The highest inhibition was recorded for P.m18, with an 85.1% reduction in biofilm formation, followed by P.m20 (80.7% inhibition), P.m14 (80.4% inhibition), and P.m12 (78.5% inhibition). The reduction in OD values after treatment suggests that ZnO-CuO nanoparticles effectively disrupted biofilm integrity, leading to a significant decrease in biofilm formation. These findings confirm the efficacy of ZnO-CuO nanoparticles in inhibiting *P. mirabilis* biofilm development and highlight their potential as alternative antimicrobial agents for controlling biofilm-associated infections.

Table 5. Effect of CuO-ZnO NPs on the gene expression of *LuxS* in the biofilm of *P. mirabilis.*

Isolate Code	Ct of *LuxS* Before Treatment with CuO-ZnO			Ct After Treatment with CuO-ZnO NPs				
	***rpo* Ct**	***LuxS* Ct**	**ΔCt**	***rpo* CT**	***LuxS* CT**	**ΔCt**	**ΔΔCt**	**Folding**
P.m12	13.73	12.32	1.41	19.96	19.15	−0.81	0.6	0.659
P.m14	10.31	10.47	0.16	12.66	12.06	−0.6	−0.76	1.693
P.m18	13.77	11.75	2.02	10.83	10.22	−0.61	1.41	0.37
P.m20	13.9	35.56	13.9	13.49	34.97	12.39	−0.27	1.20

2.8. Effect of CuO-ZnO NPs on LuxS Gene Expression

To evaluate the effects of CuO-ZnO nanocomposites on associated gene expression, RT-PCR was used. The downregulation effect was observed in four isolates (P.m12, P.m14, P.m18, and P.m20) as 0.659, 1.693, 0.37, and 1.20, respectively, while one isolate (P.m25) did not exhibit any interaction with nanocomposite stress with the folding of 1.693, as shown in Table 5. The remaining two isolates (P.m12 and P.m18) experienced a down-regulating effect with a fold change of 0.659 and 0.37 under CuO-ZnO NP stress.

The results in Figure 11 show that *LuxS* gene expression was notably ($p < 0.01$) down regulated (fold change of 0.42 ± 0.11) after CuO-ZnO nanoparticle's bacterial treatment in comparison with the control (no treatment).

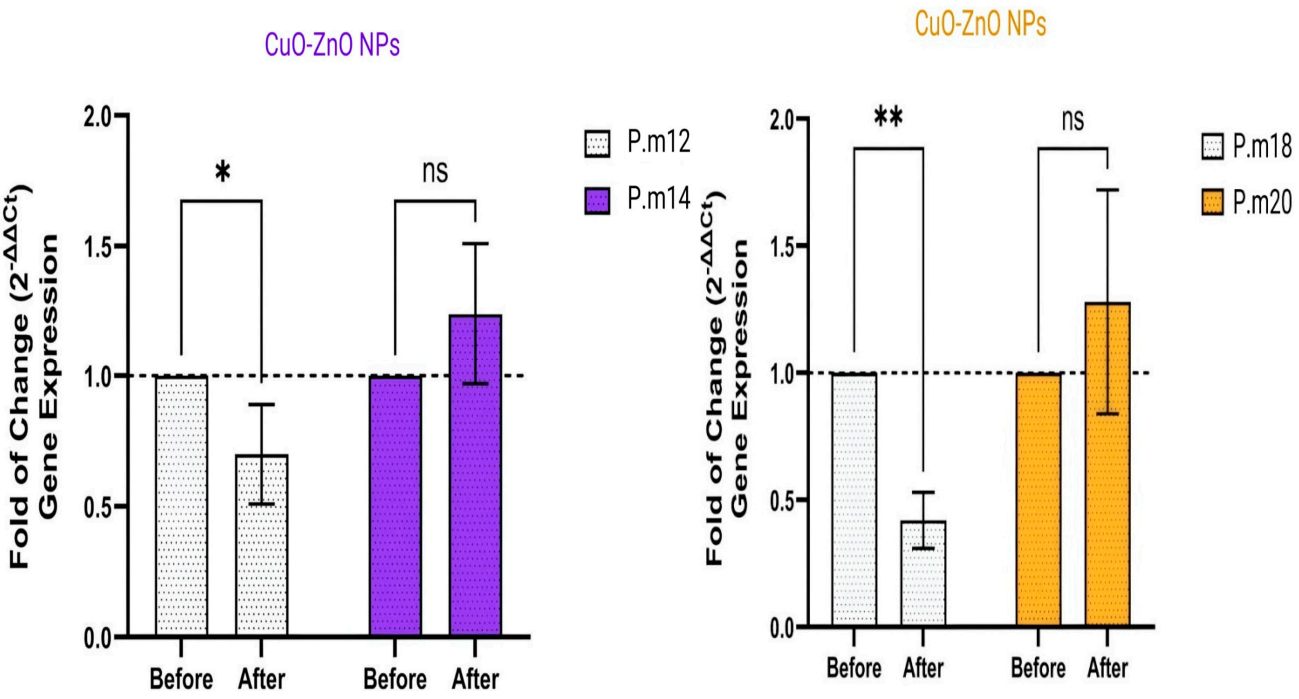

Figure 11. Mean ± SD of the fold change in *LuxS* and *rsbA* gene expression before and after treatment with CuO-ZnO nanoparticles in comparison with the untreated cells (n = 3). ns: Non-significant, *: $p < 0.05$, and ** $p < 0.01$. SD: Standard Deviation.

2.9. Discussion

Due to its numerous forms of resistance to antibiotic processes, *Proteus mirabilis*is an opportunistic pathogen that has been identified in an assortment of nosocomial and community-acquired diseases that are difficult to control [15]. *P. mirabilis* illnesses put hospitalized patients at risk of deadly outcomes. Hospitalized patients are at risk of *Proteus mirabilis* infection, which is known to cause a variety of diseases, most frequently urinary tract infections. This is especially relevant in long-stay departments that use invasive devices [16]. Increased research is essential to truly understand the seriousness of this issue and take the necessary precautions to prevent it. Similar to a different Chinese investigation, 25 out of 54 *P. mirabilis* isolates were categorized as MDR. This research demonstrates *P. mirabilis* extended-spectrum β-lactamases and develops AmpC β-lactamases, which make this bacterium a significant threat to the health of the public. The samples were obtained from humans and animals in the wild.

Nanomedicine, which has enormous potential for creating controlled systems for delivering medications to certain locations and targeting specific tissues, like infectious microbes, has received more attention in recent years. Since they have special qualities like the capacity to overcome microbial resistance, boosting antimicrobial activity against both

planktonic and biofilm-embedded microorganisms, and more, the use of nanoparticles and nanosystems based on metallic nanoparticles with antimicrobial agents attached to their surface (core–shell small systems) continues to be of interest [17]. The constraint of both chemical and physical processes for the creation of nanoparticles can be transcended by biological strategies. Because biological synthesis does not require significant amounts of chemicals, high temperatures, or a lot of time, it is quite straightforward, practical, and kinder to the environment. Because biofilm-related infections are increasingly resistant to antimicrobial treatments, they are complicated to treat. The aim of this study is to investigate how zinc oxide nanoparticles (ZnO-NPs) affect the pathological processes and antibiotic susceptibility of *S. aureus*. Recent research demonstrates ZnO-NPs' effectiveness as an anti-biofilm agent in the management of *S. aureus* infections. Based on the encouraging results reported herein, we suggest using ZnO-NPs as an addition to other antibiotics that target *S. aureus* to limit infection with this bacteria [18].

Although biological techniques are preferred because they are clean, eco-friendly, economical, safe, simple, and effective resources for high efficiency and purification, physical and conventional methods are also used to synthesize nanoparticles (NPs). This makes the green synthesis of NPs using living cells a promising and novel tool in nanotechnology [19]. Furthermore, the surface morphology of the compound exhibited a topography that is analogous to the topographies observed in high-resolution transmission electron microscopy (HR TEM) images. The presence of well-defined edges in the AFM images suggests that the samples exhibit promising reactivity characteristics [20].

CuO/MgO/ZnO nanocomposites exhibit a unique formation that enhances their photocatalytic properties, making them highly effective in degrading the organic dye Methylene Blue. The ultimate objective of this project is to develop an economical and environmentally responsible technique for eliminating harmful contaminants from industrial effluent. The results of this investigation demonstrate the produced nanoparticles' broad-spectrum dye degradation activity and well-dispersed shape [21].

The TEM images show that CuO-ZnO NPs, formed by the reduction of copper and zinc ions, are spherical in form. Metallic nanoparticles are well protected against chemical oxidation by the organic shell of the bacterial growth medium, which makes them constant and suitable for coatings or biotechnology applications [19,22].

Using a green approach, a copper oxide–zinc oxide nanocomposite and gum Arabic (GA@CuO–ZnO nanocomposite) nanocomposite were created. Based on the results of characterization, the produced nanocomposites formed stable colloidal nanosolutions, showed exceptional dispersion, and appeared at the nanoscale level. We assessed the antifungal, antibacterial, and anticancer characteristics of the bimetallic GA@CuO–ZnO copolymer [23]. It has been clarified how *P. aeruginosa* biofilms are capable of being inhibited by metal-, metal oxide-, carbon-, polymer-, hydrogel/cryogel-, and MOF-based nanocomposites. The results indicate that nanocomposites have the potential to be novel anti-biofilm agents. To validate the safety features of their application, the secure and effective use of nanocomposites should be further strengthened [24]. One study involves therapeutic techniques that combine nanotechnology with phytotherapeutics for combating pathogenic biofilms. Using *M. cymbalaria* seed extracts, we manufactured four metal oxide nanoparticles for the current investigation: silver, zinc, copper (Ag_2O, ZnO, and CuO NPs), and gold (Au NPs) [25]. Eco-friendly approaches to creating nanomaterials have received more attention recently in order to improve their biological applications and decrease hazards to human health and the environment. Numerous safe, affordable, and environmentally friendly green metal, bimetallic, and metal oxide nanoparticles with unique sizes, morphologies, and chemical compositions have been produced with the use of green nanotechnology. These nanoparticles are valued because of their great biological potential (antiviral, antibacterial, anticancer,

analgesic, anticoagulant, and biofilm inhibitory operations) and biologic compatibility [26]. Iribarnegaray et al. exploited ZnO:MgO NPs and discovered that low concentrations of the NPs inhibited *P. mirabilis* from generating biofilm. They showed that ZnO:MgO NPs stop bacteria from colonizing and settling on surfaces without forming a complete biofilm, subsequently reducing biofilm formation. Furthermore, the low concentration of ZnO:MgO NPs affects the development of the extracellular matrix, which is an essential part of the biofilm that defends bacteria from outside factors like antibiotics [27].

Among the different kinds of nanocomposites they synthesized, including ZnO–Ag_2O/Ag, ZnO–CuO, and ZnO–SnO_2 composite nanoparticles, Pandey et al. concluded that the RstA–Ag_2O nanocomposite had the best anti-QS activity when it was able to downregulate the QS PqsR and RstA genes of *Pseudomonas aeruginosa* and Acinetobacter baumannii. The in vitro study showed that the composite NPs significantly outperformed single-oxide NPs in terms of antibacterial activity, even at very low concentrations of the sample used. Interestingly, the combination of the metallic Ag/Ag_2O and ZnO structures yields the best results when used as antibacterial materials [28].

The impact of ZnO-CuO nanocomposites on quorum sensing in *Proteus mirabilis* remains largely unexplored. Our study presents one of the first investigations demonstrating biofilm inhibition and *LuxS* gene downregulation upon treatment with these nanocomposites. Previous studies on other bacteria (Pseudomonas aeruginosa and Staphylococcus aureus) have shown that metal oxide nanoparticles disrupt quorum sensing by suppressing key regulatory genes (lasI, rhlR, and lsrK). The similarity of these mechanisms suggests that ZnO-CuO nanocomposites may interfere with quorum sensing pathways in *P. mirabilis* as well. While our findings support the potential of ZnO-CuO nanocomposites as anti-biofilm agents, further studies are needed to assess dose-dependent effects and confirm whether LuxS's downregulation is specific to quorum sensing inhibition or part of a broader bacterial stress response [29].

3. Materials and Methods

3.1. Sample Collection

Urine samples were obtained from 100 patients who traveled to Al Yarmouk Teaching Hospital with infections of the urinary tract and patients of residential hospitals who had urine catheters.

Separation and recognition: VITIC 2 methodology was used to confirm the identification of *P. mirabilis*, which was primarily achieved through inoculation on blood agar and MacConkey substrate at a temperature of 37 °C for twenty-four hours.

3.2. Antibiotic Susceptibility Test

CLSI 2021 indicates that the disk method was employed to test for susceptibility on the Mueller–Hinton agar plates. Gentamicin 10 µg, Ampicillin 25 µg, Levofloxacin 5 µg, Ciprofloxacin 15 µg, Cefoxitin 30 µg, Ticarcilline + Clavulanic acid µg, Cefepimeµg, Piperacillin–Tazobactam 100/10 µg, and Nitrofurnation 300 µg were the antibiotics that were employed.

3.3. Production of Biofilm Using the Colorimetric Microtiter

The biofilm-forming ability of *P. mirabilis* isolates was assessed using a colorimetric microtiter plate assay with crystal violet staining.

For biofilm formation, bacterial cultures were grown in brain heart infusion (BHI) broth supplemented with 1% glucose to enhance adherence. The inoculum was prepared by adjusting overnight bacterial cultures to an OD_{600} of 0.1, followed by a 1:100 dilution in fresh medium. A 200 µL aliquot of the diluted culture was added to each well of a

96-well flat-bottom microtiter plate. For negative controls, the wells contained only BHI with 1% glucose without bacterial inoculation.

The plates were incubated under static conditions at 35–37 °C for 24–30 h. After incubation, the wells were gently washed three times with phosphate-buffered saline (PBS, pH 7.2) to remove non-adherent cells. The remaining attached biofilm was fixed using methanol (150 µL/well) for 15 min and air-dried at room temperature. The biofilms were then stained with 150 µL of 0.1% crystal violet for 15 min, followed by three washes with PBS to remove excess dye.

To quantify biofilm formation, the retained stain was solubilized using 150 µL of 95% ethanol, and the plate was incubated for 30 min at room temperature without shaking. The optical density (OD) was measured at 630 nm using a microtiter plate reader (GloMax, Promega Hollow Road Madison, Fitchburg, WI, USA).

The biofilm-forming ability of the isolates was classified based on OD readings as follows:

No biofilm: $OD \leq ODc$

Weak biofilm: $ODc < OD \leq 2 \times ODc$

Moderate biofilm: $2\times ODc < OD \leq 4 \times ODc$

Strong biofilm: $OD > 4 \times ODc$

The cut-off OD (ODc) was calculated as the mean OD of the negative control wells + (3 × standard deviation of the negative control OD values).

3.4. Preparation of Bacterial Suspension

In a non-shaking incubator, *P. mirabilis* was maintained in brain heart broth (250 mL) at 37 °C for 24 h. This bacterial broth was then centrifuged, the supernatant was extracted, and the residue was discarded.

3.5. Synthesis of CuO-ZnO Nanoparticles

In the present study, copper (II) acetate ($Cu(CH_3COO)_2 \cdot H_2O$) and zinc acetate ($Zn(O_2CCH_3)_2$) were used as precursor materials for the biosynthesis of ZnO-CuO nanocomposites. This study aimed to synthesize copper oxide–zinc oxide nanocomposites using a biological method from multidrug-resistant (MDR) *Proteus mirabilis*, a strong biofilm producer.

The biosynthesis process involves both intracellular and extracellular mechanisms. In intracellular synthesis, positively charged metal ions are attracted to the negatively charged bacterial cell membrane due to electrostatic interactions. Within the bacterial cell, specific enzymes act as bioreductants, reducing the metal ions to nanoscale particles. In extracellular synthesis, the bacterial cells secrete reductase enzymes that facilitate the extracellular reduction of metal ions, leading to the formation of nanoparticles outside the cell. This biogenic approach enhances nanoparticle stability, promotes environmentally friendly synthesis, and minimizes the toxic byproducts associated with conventional chemical synthesis methods, making it a sustainable and efficient strategy for nanomaterial production.

For nanoparticle synthesis, the precipitation method was used. A 200-milliliter filtrate of *P. mirabilis* broth was mixed with 10 g of zinc acetate and 10 g of copper (II) acetate, with the temperature maintained at 37 °C. The mixture was sealed in a dark plastic bag and incubated in a shaker for 24 h. Following incubation, the mixture was centrifuged, and the precipitate was collected. A three-step washing process using deionized water was performed to remove any residual impurities. The formation of CuO-ZnO nanoparticles was visually confirmed by a color change in the reaction mixture, indicating successful nanoparticle synthesis. The obtained precipitate was air-dried and stored under dry conditions for further characterization and evaluation [13] (Figure 12).

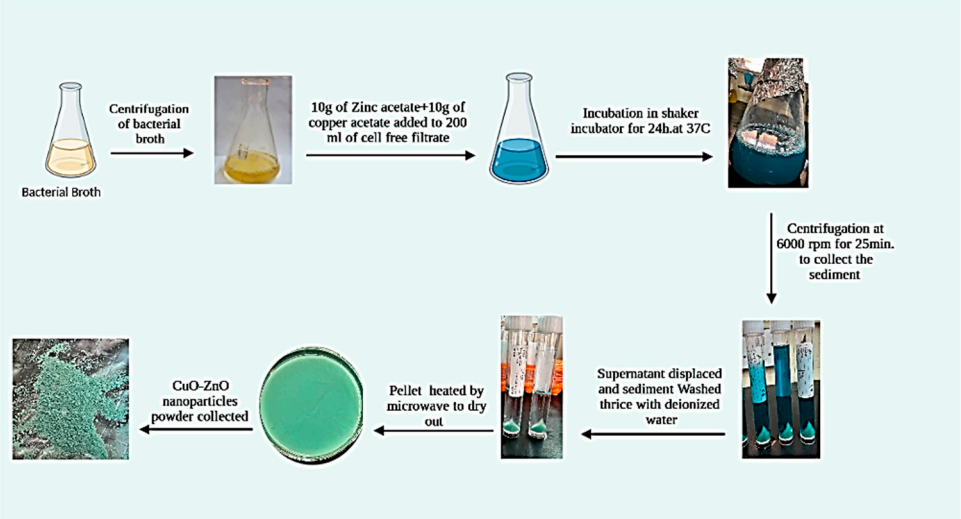

Figure 12. Biosynthesis process of CuO-ZnO nanocomposites.

3.6. Characterization of CuO-ZnO Nanocomposites

Understanding the properties of nanostructures requires characterization. The physical characteristics of NPs were ascertained using the following techniques: SEM and TEM were employed to ascertain sizes and shapes; UV-Vis (UV-DRS) was utilized to examine the visual characteristics of the materials; and Atomic Force Microscopy (AFM) was applied to measure the volume and height of the nanoparticles in 3D vision. XRD is a materials science technique that establishes a material's crystallographic structure and energy-dispersive X-ray spectrometry (EDX) confirms the presence of essential components in the prepared sample [30].

3.6.1. UV-Visible (UV-VIS) Spectral Analysis

The formation of nanoparticles was confirmed by measuring the wavelength of the reaction mixture in the UV-VIS spectrum of a Perkin Elmer spectrophotometer at a resolution of 1 nm in a 2 mL quartz cuvette with a 1 cm path length. The scanning range for the samples was 200–900 nm at a scan speed of 500 nm/min, with a blank reference used for correction of the spectrophotometer. The UV-Vis absorption spectra of all of the samples were recorded and the numerical data were plotted. This examination was carried out in the laboratories of the Department of Chemistry, College of Sciences, University of Baghdad.

3.6.2. Atomic Force Microscopy (AFM) Analysis

Atomic Force Microscopy was used to analyze the average diameter of the synthesized nanoparticles. A thin film of the prepared NPs was deposited on a silica glass plate by dropping a few drops of the NPs on the plate and allowing them to dry at room temperature in the dark. The deposited film glass plate was then scanned via AFM. This examination was conducted in the laboratories of the Department of Chemistry, College of Sciences, University of Al-Nahrain.

3.6.3. X-Ray Diffraction (XRD) Method Analysis

The crystal structure of the NPs was measured via X-ray diffraction (XRD). The powdered sample was prepared for XRD analysis via grinding, which can be accomplished by several different methods, depending on the sample matrix, the size of the sample, and/or the quantity of prepared material needed. The best-used method is sample slurry/smear

slide mount for small sample amounts. The samples were sent as powder to a research center in Tehran, Iran.

3.6.4. Transmission Electron Microscope (TEM Analysis)

To study the morphology and size of the NPs, a transmission electron microscope (TEM) was used for investigation. For TEM imaging, the NP suspensions in the absence or presence of anesthetics were deposited on the specimen grids and absorbed for 1 min. The excess solution was removed with filter paper, and the samples were air-dried. The samples were sent as powder to a research center in Tehran, Iran

3.6.5. Field Emission Scanning Electron Microscope (FESEM)

A field emission scanning electron microscope (FESEM) was used to study the morphology of the synthesized nanoparticles. The electron beams the focus of the sample to generate images by scanning the surface. The electrons interfere with the atoms in the sample, generating various signals that include surface topography. In a raster scan pattern, the electron beam is scanned, and the beam position is combined with the detected signal to create the image. The FESEM analysis was carried out at the Alkhura Nano-Science Center, Alyarmouk/Baghdad, Iraq.

3.6.6. Energy-Dispersive X-Ray (EDX)

EDX analysis determines the concentrations of the constituent elements and their composition through scanning with an electron microscope. EDX was used to ascertain elemental selenium in solid samples. This process was performed by using a BRUKER Q200 (Germany). It is based on the "fingerprint" energies of the X-rays emitted by the samples during the bombardment of an electron beam. It is also possible to perform a general mapping of the sample by executing the X-ray spectra in scan mode. This examination was conducted in the laboratories of the Department of Physics, College of Sciences, University of Al-Nahrain.

3.7. Determination of the MinimumInhibitory Concentration (MIC) of CuO-ZnO Nanoparticles

A technique called microdilution was used to determine the minimum inhibitory concentrations (MICs) in the culture broth, and the antibacterial activity of each produced nanoparticle was evaluated. Additional dilutions were made with doses of around 512 and 2 μg/mL. In short, the 96-well microtiter plate was filled with 125 μL of sterile Mueller–Hinton broth in the first column and 125 μL in the remaining wells. The first column of the microtiter plate was subsequently populated with 125 μL of the respective nanoparticle solution in PBS (100 μg/mL) and mixed with the medium, resulting in a concentration of 50 mg/mL of CuO-ZnO NPs. Next, 125 μL was then systematically transferred to the remaining wells, discarding 125 μL of the mixture in the last column, until each well had a final volume of 125 μL. 2.5 μL of the overnight culture (9×10^8 CFU/mL)of modified pathogenic bacteria isolates which was then placed in each well. After being covered, the microtiter plates were incubated for twenty-four hrs at 37 °C [31].

3.8. CuO-ZnO Nanocomposite's Effect on the Formation of Biofilm

A 96-well microtiter plate was utilized for this assay, which was completed by 12 h. The tested isolates were cultivated in brain heart infusion broth for 24 h at 37 °C. Each benefited from 100 mL of bacterial inoculum that had been adjusted to 0.5 McFarland standard. Each well contained 100 mL of nanocomposite remedy at a sub-inhibitory concentration. The tubes were then incubated at 37 °C for 48 h. Clear broth was utilized as the negative control, whilst a bacterial culture devoid of nanoformulations served as the positive control. Following incubation, the contents of each well were disposed of, and the

sterile saline micro-plate was washed three times before being dried for forty-five minutes at sixty degrees Celsius. After staining with 200 mL of 0.1% crystal violet and letting it sit for 15 min at room temperature, the microplate was washed again using normal sterile saline. Next, 200 mL of 30% acetic acid was added to each well, and a microtiter plate reader was utilized to find the OD (optical density) at 630 nm for each well [28].

3.9. RT-qPCR Protocol

The retrieved genomic DNA was synthesized by a heated cycler (Thermo Fisher Scientific, USA) to detect the existence of rpo and *LuxS* of *P. mirabilis* (Table 6). The cDNA synthesis process was carried out in two steps. The first step involved generating cDNA from RNA using a Protoscript cDNA synthesis kit, following the manufacturer's recommended protocol. Specific primers for rpo (housekeeping gene) and *LuxS* transcripts were used for amplification. For each sample, three PCR tubes were prepared: one for the *LuxS* gene, one for the rpo gene, and one for the negative control. A 20 µL reaction mixture was prepared for cDNA synthesis, consisting of 10 µL of Luna Universal Master Mix, 1 µL of forward primer, 1 µL of reverse primer, 5 µL of RNA template, and 3 µL of nuclease-free water. The reaction was performed under standard cycling conditions for reverse transcription. In the second step, cDNA from both the control and the treated isolates was collected simultaneously for quantitative estimation using SYBR Green fluorescence detection. The expression levels of the *LuxS* gene were normalized using rpo as the reference gene, and data were analyzed accordingly. The component's reaction mix and quantity are provided in Table 6 below.

Table 6. Primers utilized in this work.

Primer		Sequence	Product Size (bp)	Reference
luxS	F	5′-TTCGCCAATGGGATGTCGTA-3′	474	[32] (Wasfiet al., 2020)
	R	5′-TCCATAGCTGCCTTCCATGC-3′		
rpoA	F	5′-GCGTGTTATAGCCCAGTTGA-3′	945	[33] (Saleh et al., 2019)
	R	5′-AGGCTGACGAACATCACGTA-3′		

For each gene, the difference in cycle thresholds (CTs) and fold changes among the calibrators and treatment groups was determined. The data were then normalized by employing the rpo values. After examining PCR tubes and collecting the liquid for 1 m at 2000 g, the real-time PCR application was set up using the prescribed thermocycling methodology. The Livak algorithm esd applied to collect and analyze the data. Expression levels were ascertained through the use of relative quantification [34].

3.10. Gene Expression Calculation

Expression levels were assessed through relative quantification. For each gene, the difference in cycle levels (ΔCt) and fold changes among the three treatment groups and the calibrators were evaluated (Livak and Schmittgen, 2001) [35].

The quantitative real-time PCR (qRT-PCR) reaction was carried out using a structured thermal cycling program. The process began with a reverse transcription and enzyme activation step at 37 °C for 15 min, followed by an initial denaturation step at 95 °C for 10 min. The amplification cycles included denaturation at 95 °C for 15 s, annealing at 50 °C, 58 °C, or 60 °C for 30 s, and extension at 72 °C for 30 s. A total of 40 amplification cycles were performed. To ensure the specificity of the amplified products, a melting curve

analysis was conducted by gradually increasing the temperature from 72 °C to 95 °C at a rate of 0.3 °C per second. These values were calibrated to rpoA for *P. mirabilis* expression:

$$\text{Folding} = 2^{-\Delta\Delta CT} \quad (1)$$

$$\text{Gene expression} = 2^{-\Delta Ct} \quad (2)$$

$$\Delta\Delta Ct = \Delta Ct \text{ Treated (T)} - \Delta Ct \text{ Untreated (C)} \quad (3)$$

$$\Delta Ct = Ct \text{ of the target gene} - Ct \text{ of the housekeeping gene}\ldots \text{ Untreated} \quad (4)$$

$$\Delta Ct = Ct \text{ of the target gene} - Ct \text{ of the housekeeping gene}\ldots. \text{ Treated} \quad (5)$$

A less than two-fold change was regarded as irrelevant. A melting curve was obtained from the 72 °C to 95 °C temperature range at 0.3 °C/s.

3.11. Anti-Cancer Activity of CuO-ZnO Nanocomposites

3.11.1. Determination of Cell Viability

In a 96-well microtiter plate, 4000 cells per well were utilized to investigate the cytotoxic effect of CuO/ZnO NPs synthesized from *P. mirabilis* using MTT ready-to-use Kit contents 13, UBC-40, and HdFn cell lines. The HdFn cell line was prepared at the Biotechnology Research Center of Al-Nahrain University, Baghdad, Iraq.

The medium used to grow the cells was altered to a new medium with various quantities of nanocomposites (25, 50, 100, 200, and 400 µg/mL) to treat both cell lines after a 12-h incubation period. The cells were grown using the provided medium at 37 °C, in keeping with the providers' instructions. To determine the intensity at 450 nm, a Bio-Tek microplate reader (College Park, GA, USA) was employed. Curves were generated with GraphPad Prism 7 software from GraphPad Software, Inc., San Diego, CA, USA, in a dose-dependent manner [36].

3.11.2. Cytotoxicity Assay

The in vitro method was employed to investigate the possible cytotoxic effect of biosynthesized nanoparticles on tumor cell lines (UBC40) and normal cell lines (HDFn).

Cytotoxic effects were assessed using an in vitro 3-(4,5-dimethylthiazol-2-yl)-2,5-diphenyltetrazolium bromide (MTT) assay [37].

A total of 7000 cells were seeded in each well of a 96-well plate and incubated overnight to ensure cell adhesion. The cell lines (UBC-40) were then exposed to increasing concentrations of compounds (25–400 µg/mL); three replicate wells were used for each treatment. Following incubation (24 h), the medium was removed from the plate, and a 20 µL MTT solution (5 mg/mL) (Shanghai Macklin Biochemical Co., Ltd., Shanghai, China) was added to each well and incubated for 3 h at 37 °C in the dark. To dissolve the MTT, 50 µL DMSO (Bio Basic Inc., Amherst, NY, USA) was added, followed by 10 min of shaking [38]. A microplate reader (BioTek Instruments, Inc., Santa Clara, CA, USA) was used to measure the absorbance at 490 nm. The following equation was used to determine the percentage of viable cells from the raw absorbance data:

$$\text{Viability \%} = (\text{A test} - \text{A blank})/(\text{A control} - \text{A blank}) \times 100$$

where 'A' represents the absorbance. The dose–response curve was generated using GraphPad Prism software version 6 (Dotmatics), and the growth inhibitory concentration that reduces viability by 50% (GI50) was determined via the same curve [39]. The experiments were carried out in triplicate, and the mean and standard deviation were used to express the findings. The T test was used to determine how the research factors affected the biofilm.

Software called SPSS version 26 was used to perform these statistical analyses. When $p < 0.05$, the differences were deemed significant.

4. Conclusions

ZnO-CuO nanocomposites were successfully synthesized using a green chemistry approach and characterized using FT-IR, UV-Vis, DLS, SEM, XRD, TEM, AFM, and BET techniques. These characterization methods provided valuable insights into the structural and morphological properties of the nanoparticles, demonstrating their potential for biomedical and industrial applications. This study specifically investigated the anti-biofilm properties of ZnO-CuO nanoparticles against *Proteus mirabilis* and demonstrated their significant inhibitory effects on biofilm formation. While previous research has explored the antimicrobial potential of various green synthesized nanoparticles, our findings contribute new insights into the quorum-sensing regulation and biofilm inhibition mechanisms of ZnO-CuO nanocomposites. The successful development of these nanoparticles through an environmentally friendly, high-yield, and low-cost process highlights their potential as surface-coating antibacterial agents for medical applications. However, further studies are needed to evaluate their effects on other bacterial species and to optimize their applications in biomedical devices for preventing biofilm-associated infections. Future studies will also focus on evaluating the dose–response relationship of ZnO-CuO nanoparticles on *P. mirabilis* biofilm inhibition by testing a range of concentrations to determine the optimal inhibitory dose.

Author Contributions: Formal analysis, M.E.A., N.H.F. and H.H.A.; funding acquisition, M.W.A.; investigation, M.E.A., N.H.F. and H.H.A.; methodology, M.E.A., N.H.F., H.H.A. and M.W.A.; project administration, M.W.A.; software, N.H.F.; supervision, M.W.A.; writing—original draft, M.E.A. and M.W.A.; writing—review and editing, M.E.A., N.H.F., H.H.A. and M.W.A. All authors have read and agreed to the published version of the manuscript.

Funding: Deanship of Scientific Research, Vice Presidency for Graduate Studies and Scientific Research, King Faisal University, Saudi Arabia.

Data Availability Statement: The original contributions presented in this study are included in the article. Further inquiries can be directed to the corresponding author.

Acknowledgments: This work was supported by the Deanship of Scientific Research, Vice Presidency for Graduate Studies and Scientific Research, King Faisal University, Saudi Arabia (Project No: KFU250576).

Conflicts of Interest: The authors declare that they have no known competing financial interests or personal relationships that could have appeared to have influenced the work reported in this paper.

References

1. Ragupathi, H.; Pushparaj, M.M.; Gopi, S.M.; Govindarajan, D.K.; Kandaswamy, K. Biofilm matrix: A multifaceted layer of biomolecules and a defensive barrier against antimicrobials. *Arch. Microbiol.* **2024**, *206*, 432. [CrossRef] [PubMed]
2. Flemming, H.C.; van Hullebusch, E.D.; Neu, T.R.; Nielsen, P.H.; Seviour, T.; Stoodley, P.; Wingender, J.; Wuertz, S. The biofilm matrix: Multitasking in a shared space. *Nat. Rev. Microbiol.* **2023**, *21*, 70–86. [CrossRef] [PubMed]
3. Balaure, P.C.; Grumezescu, A.M. Recent advances in surface nanoengineering for biofilm prevention and control. Part II: Active, combined active and passive, and smart bacteria-responsive antibiofilm nano-coatings. *Nanomaterials* **2020**, *10*, 1527. [CrossRef]
4. Abbas, H.M.; Al Marjani, M.F.; Gdoura, R. Evaluation of the antibacterial activity of CuO and ZnO nanoparticles against uropathogenic *Escherichia coli*. *J. Taibah Univ. Sci.* **2024**, *18*, 2322776. [CrossRef]
5. Mancuso, G.; Midiri, A.; Gerace, E.; Marra, M.; Zummo, S.; Biondo, C. Urinary Tract Infections: The Current Scenario and Future Prospects. *Pathogens* **2023**, *12*, 623. [CrossRef]
6. Kumar, J.A.; Krithiga, T.; Manigandan, S.; Sathish, S.; Renita, A.A.; Prakash, P.; Prasad, B.N.; Kumar, T.P.; Rajasimman, M.; Hosseini-Bandegharaei, A.; et al. A focus to green synthesis of metal/metal based oxide nanoparticles: Various mechanisms and applications towards ecological approach. *J. Clean. Prod.* **2021**, *324*, 129198. [CrossRef]

7. El-Naggar, N.E.; El-Sawah, A.A.; Elmansy, M.F.; Elmessiry, O.T.; El-Saidy, M.E.; El-Sherbeny, M.K.; Sarhan, M.T.; Elhefnawy, A.A.; Dalal, S.R. Process optimization for gold nanoparticles biosynthesis by *Streptomyces albogriseolus* using artificial neural network, characterization and antitumor activities. *Sci. Rep.* **2024**, *14*, 4581. [CrossRef]
8. Chang, T.; Li, Z.; Yun, G.; Jia, Y.; Yang, H. Enhanced photocatalytic activity of ZnO/CuO nanocomposites synthesized by hydrothermal method. *Nano-Micro Lett.* **2013**, *5*, 163–168. [CrossRef]
9. Das, S.; Srivastava, V.C. An overview of the synthesis of CuO-ZnO nanocomposite for environmental and other applications. *Nanotechnol. Rev.* **2018**, *7*, 267–282. [CrossRef]
10. Ivask, A.; Bondarenko, O.; Jepihhina, N.; Kahru, A. Profiling of the reactive oxygen species-related ecotoxicity of CuO, ZnO, TiO_2, silver and fullerene nanoparticles using a set of recombinant luminescent Escherichia coli strains: Differentiating the impact of particles and solubilised metals. *Anal. Bioanal. Chem.* **2010**, *398*, 701–716. [PubMed]
11. Hu, Y.; Ruan, X.; Lv, X.; Xu, Y.; Wang, W.; Cai, Y.; Ding, M.; Dong, H.; Shao, J.; Yang, D.; et al. Biofilm microenvironment-responsive nanoparticles for the treatment of bacterial infection. *Nano Today* **2022**, *46*, 101602. [CrossRef]
12. Jaffar, N.; Miyazaki, T.; Maeda, T. Biofilm formation of periodontal pathogens on hydroxyapatite surfaces: Implications for periodontium damage. *J. Biomed. Mater. Res. A* **2016**, *104*, 2873–2880. [CrossRef] [PubMed]
13. Widiarti, N.; Sae, J.K.; Wahyuni, S. Synthesis CuO-ZnO nanocomposite and its application as an antibacterial agent. In *IOP Conference Series: Materials Science and Engineering*; IOP Publishing: London, UK, 2017; Volume 172, p. 012036.
14. Abdelghafar, A.; Yousef, N.; Askoura, M. Zinc oxide nanoparticles reduce biofilm formation, synergize antibiotics action and attenuate *Staphylococcus aureus* virulence in host; an important message to clinicians. *BMC Microbiol.* **2022**, *22*, 244. [CrossRef] [PubMed]
15. Hafiz, T.A.; Alghamdi, G.S.; Alkudmani, Z.S.; Alyami, A.S.; AlMazyed, A.; Alhumaidan, O.S.; Mubaraki, M.A.; Alotaibi, F.E. Multidrug-resistant *Proteus mirabilis* infections and clinical outcome at tertiary hospital in Riyadh, Saudi Arabia. *Infect. Drug Resist.* **2024**, *17*, 571–581. [CrossRef]
16. Skłodowski, K.; Chmielewska-Deptuła, S.J.; Piktel, E.; Wolak, P.; Wollny, T.; Bucki, R. Metallic Nanosystems in the Development of Antimicrobial Strategies with High Antimicrobial Activity and High Biocompatibility. *Int. J. Mol. Sci.* **2023**, *24*, 2104. [CrossRef]
17. Hemdan, B.A.; El-Naggar, M.E.; Abd-Elgawad, S.E.; El Zawawy, N.A.; Mahmoud, Y.A.G. Bacterial cell-free metabolites-based zinc oxide nanoparticles for combating skin-causing bacterial infections. *Biomass Convers. Biorefin.* **2023**, *13*, 23381–23394. [CrossRef]
18. ElTaweel, M.; Said, H.S.; Barwa, R. Emergence of extensive drug resistance and high prevalence of multidrug resistance among clinical *Proteus mirabilis* isolates in Egypt. *Ann. Clin. Microbiol. Antimicrob.* **2024**, *23*, 46. [CrossRef] [PubMed]
19. Salem, S.S.; Fouda, A. Green synthesis of metallic nanoparticles and their prospective biotechnological applications: An overview. *Biol. Trace Elem. Res.* **2021**, *199*, 344–370. [CrossRef]
20. Ali, L.H.; Muslim, W.A.; Ghali, A.A.; Salem, K.H.; Mohammed, K.A.; Zabibah, R.S.; Alkhafaji, M.A.; Elayaperumal, M.; Ameen, N.I.; Saxena, K.K. Biosynthesis of Au–CuO–ZnO Nanocomposite using leaf extract and activity as anti-bacterial, anti-cancer, degradation of CB dye. *J. Mater. Sci. Mater. Electron.* **2023**, *34*, 1087. [CrossRef]
21. Imran, M.; Raza, M.; Noor, H.; Faraz, S.M.; Raza, A.; Farooq, U.; Khan, M.E.; Ali, S.K.; Bakather, O.Y.; Ali, W.; et al. Insight into mechanism of excellent visible-light photocatalytic activity of CuO/MgO/ZnO nanocomposite for advanced solution of environmental remediation. *Chemosphere* **2024**, *359*, 142224. [CrossRef]
22. Serouti, A.; Eddine, L.S.; Meneceur, S.; Hasan, G.G.; Mohammed, H.A.; Salmi, C.; Iman, K.; Ferhat, M.F.; Ali, O.B.; Abdullah, J.A.A. Biogenic ZnO/CuO/Fe_2O_3 Nanocomposite: A Groundbreaking Approach for Enhanced Degradation Capabilities and Reusability in Dye Removal Applications. *Arab. J. Sci. Eng.* **2024**, *49*, 753–764. [CrossRef]
23. El-Sayyad, G.S.; El-Sayed, E.S.R.; Rizk, S.H.; Abdel-Maksoud, M.A.; Zakri, A.M.; Malik, A.; Hashem, A.H. An eco-friendly and cost-effective approach for the synthesis of a novel GA@CuO–ZnO nanocomposite: Characterization, antimicrobial and anticancer activities. *RSC Adv.* **2025**, *15*, 513–523. [CrossRef] [PubMed]
24. Omran, B.A.; Tseng, B.S.; Baek, K.H. Nanocomposites against *Pseudomonas aeruginosa* biofilms: Recent advances, challenges, and future prospects. *Microbiol. Res.* **2024**, *279*, 127656. [CrossRef] [PubMed]
25. Mathimaran, A.; Pandian, C.J.; Sappanimuthu, P.; Kirshnakumar, H.; Amala, M.; Veerapandiyan, M.; Kingsly, J.; Solomon, A.; Sonamuthu, J.; Jeyaraman, J. Synthesis of multifunctional silver oxide, zinc oxide, copper oxide and gold nanoparticles for enhanced antibacterial activity against ESKAPE pathogens and antioxidant, anti-cancer activities using *Momordica cymbalaria* seed extract. *Mater. Today Commun.* **2024**, *39*, 108838. [CrossRef]
26. Dubey, S.; Virmani, T.; Yadav, S.K.; Sharma, A.; Kumar, G.; Alhalmi, A. Breaking Barriers in Eco-Friendly Synthesis of Plant-Mediated Metal/Metal Oxide/Bimetallic Nanoparticles: Antibacterial, Anticancer, Mechanism Elucidation, and Versatile Utilizations. *J. Nanomater.* **2024**, *2024*, 9914079. [CrossRef]
27. Iribarnegaray, V.; Navarro, N.; Robino, L.; Zunino, P.; Morales, J.; Scavone, P. Magnesium-doped zinc oxide nanoparticles alter biofilm formation of *Proteus mirabilis*. *Nanomedicine* **2019**, *14*, 1551–1564. [CrossRef]

28. Pandey, M.; Singh, M.; Wasnik, K.; Gupta, S.; Patra, S.; Gupta, P.S.; Pareek, D.; Chaitanya, N.S.N.; Maity, S.; Reddy, A.B.; et al. Targeted and enhanced antimicrobial inhibition of mesoporous ZnO–Ag2O/Ag, ZnO–CuO, and ZnO–SnO_2 composite nanoparticles. *ACS Omega* **2021**, *6*, 31615–31631. [CrossRef] [PubMed]
29. Karrari, S.; Mohammadzadeh, H.; Jafari, R. Characterization of ZnO-CuO and ZnO-CuO-NiO nanocomposites prepared by co-precipitation and antibacterial properties. *Appl. Phys. A* **2025**, *131*, 147. [CrossRef]
30. Siddiqui, H.; Qureshi, M.S.; Haque, F.Z. Biosynthesis of flower-shaped CuO nanostructures and their photocatalytic and antibacterial activities. *Nano-Micro Lett.* **2020**, *12*, 1–11. [CrossRef] [PubMed]
31. Rasheed, E.A.; Hamid, M.K.; Ahmed, M.E. A Green Synthesized of Zinc Oxide Nanoparticles Against MRSA Wound Healing In Vivo. *J. Nanostruct.* **2023**, *13*, 989–998. [CrossRef]
32. Wasfi, R.; Abdellatif, G.R.; Elshishtawy, H.M.; Ashour, H.M. First time characterization of viable but non culturable *Proteus mirabilis*: Induction and resuscitation. *J. Cell. Mol. Med.* **2020**, *24*, 2791–2801. [CrossRef] [PubMed]
33. Saleh, T.H.; Hashim, S.T.; Malik, S.N.; AL-Rubaii, B.A.L. Down-regulation of *flil* gene expression by Ag nanoparticles and TiO_2 nanoparticles in pragmatic clinical isolates of *Proteus mirabilis* and *Proteus vulgaris* from urinary tract infection. *Nano Biomed. Eng.* **2019**, *11*, 321–332. [CrossRef]
34. Mahdi, S.M.; Ahmed, M.E.; Abbas, A.F. Effect of Enterococcin–Zinc Oxide Nanoparticles on Gene Expression of *rsbA* Swarming Genes in *Proteus mirabilis* Isolation Catheter Urine. *Biomed. Pharmacol. J.* **2024**, *17*, 1249–1264. [CrossRef]
35. Livak, K.J.; Schmittgen, T.D. Analysis of Relative Gene Expression Data Using Real-Time Quantitative PCR and the $2^{-\Delta\Delta CT}$ Method. *Methods* **2001**, *25*, 402–408. [CrossRef] [PubMed]
36. Kadhim, Z.H.; Ahmed, M.E.; Şimşek, İ. Biologically synthesized Copper Nanoparticles from *S. epidermidis* on resistant *S. aureus* and cytotoxic assay. *Bionatura* **2023**, *8*, 1–10. [CrossRef]
37. Zaki, N.H.; Ali, A.M.; Al-Rubaiee, G.H.; Alhammer, A.H. Anti-bacterial and Anti-tumoral Activities of *Spirulina platensis* Extracellular Extract. *Malays. J. Med. Health Sci.* **2022**, *18*, 11–16.
38. Ali, S.M.; Al-Karam, L.Q.; Alhammer, A.J.N. In Vitro Cancer Cells Therapy with Nano-gold Depending on its Optical Properties. *NeuroQuantology* **2022**, *20*, 57. [CrossRef]
39. Lafta, F.M.; Mohammed, R.K.; Alhammer, A.H.; Ahmed, M.E. Cytotoxic Potential of Neem (Azadirachtaindica A. Juss) Oil. *Trop. J. Nat. Prod. Res. (TJNPR)* **2023**, *7*, 5436–5440.

Disclaimer/Publisher's Note: The statements, opinions and data contained in all publications are solely those of the individual author(s) and contributor(s) and not of MDPI and/or the editor(s). MDPI and/or the editor(s) disclaim responsibility for any injury to people or property resulting from any ideas, methods, instructions or products referred to in the content.